Eddy-Zonal Flow Interactions and the Persistence of the Zonal Index

EDWIN P. GERBER[1] AND GEOFFREY K. VALLIS[2]

[1]*Applied Physics and Applied Mathematics, Columbia University*

[2]*GFDL, Princeton University*

Journal of the Atmospheric Sciences

Corresponding Author: Edwin P. Gerber, epg2108@columbia.edu

Submitted, 15 June 2006

Revised, 21 November 2006

Abstract

An idealized atmospheric general circulation model is used to investigate the factors controlling the timescale of intraseasonal (10-100 day) variability of the extratropical atmosphere. Persistence on these timescales is found in patterns of variability that characterize meridional vacillations of the extratropical jet. Depending on the degree of asymmetry in the model forcing, patterns take on similar properties to the zonal index, annular modes, and North Atlantic Oscillation. It is found that the timescale of jet meandering is distinct from the obvious internal model timescales, suggesting that interaction between synoptic eddies and the large scale flow establish a separate, intraseasonal timescale. A mechanism is presented by which eddy heat and momentum transport couple to retard motion of the jet, slowing its meridional variation and thereby extending the persistence of zonal index and annular mode anomalies. The feedback is strong and quite sensitive to model parameters when the model forcing is zonally uniform. However, the timescale of jet variation drops and nearly all sensitivity to parameters is lost when zonal asymmetries, in the form of topography and thermal perturbations that approximate land-sea contrast, are introduced. A diagnostic on the zonal structure of the zonal index provides intuition on the physical nature of the index and annular modes, and hints at why zonal asymmetries limit the eddy-mean flow interactions.

1. Introduction

In this paper we investigate processes that determine the persistence of the zonal index and North Atlantic Oscillation (NAO), focusing on intraseasonal timescales. By intraseasonal, we mean timescales of 10–100 days, longer than those associated with synoptic variability, but not so long as to allow for significant changes in the boundary conditions or forcing, such as sea surface temperature. On these shorter periods, then, the focus is on internal processes in the atmosphere that extend the persistence of these large scale patterns beyond synoptic timescales. Variability in this range may account for all, or at least a large fraction, of the variability of the NAO and zonal index on interannual timescales (e.g. Feldstein 2000a,b).

The zonal index as a measure of the strength of the zonally averaged circulation dates back at least to Rossby (1939), though it was not until somewhat later that it was understood that the index more accurately describes *latitudinal* variations of the jet (e.g. Namias 1950). It has become conventional to define the index as the principal component time series associated with the first EOF of the zonally averaged zonal wind (e.g. Feldstein 2000a; Lorenz and Hartmann 2001). It is closely related to the so-called annular mode index, associated with the first Empirical Orthogonal Function (EOF) of sea level pressure (Thompson et al. 2000), and the NAO index, which is typically determined from rotated EOF analysis of pressure or geopotential surfaces (e.g Barnston and Livezey 1987). To leading order, the zonal and annular mode indices characterize meridional shifts of the extratropical jet, with the implication of hemispheric scale variation, while the NAO suggests a more limited zonal scale of jet variation, with focus restricted to the North Atlantic region. Variability in this sector dominates the zonal average, however, so the NAO index highly correlated with the more zonal measures. All these indices essentially describe slow meanderings of

the extratropical jet, and it is the timescale of these variations that is the subject of this study. We investigate the dynamics controlling variability of the zonally average jet and the influence of large scale zonal asymmetries on the zonally averaged flow.

The zonal index and NAO exhibit considerable energy on intraseasonal timescales. Anomalies of the jet persist longer than typical baroclinic eddies; during the Northern Hemisphere winter, the e-folding timescales of the zonal index, annular mode, and NAO are 18, 10.6, and 9.5 days, respectively (Feldstein 2000a,b). They show no pronounced spectral peak at any frequency, however, exhibiting a relatively white spectrum at low frequencies. The stochastically stirred barotropic model of Vallis et al. (2004) provides perhaps the simplest explanation for both the persistence and flat spectrum of the patterns. There it is shown that annular mode and NAO-like patterns may simply be driven by random variations in the eddy vorticity fluxes. As the integral of eddy fluxes, the zonal flow exhibits greater power on lower frequencies than the eddies. If one assumes that the eddy fluxes are white in time (at least on timescales longer than 10 days) and that the damping of the large scale anomalies is linear, the NAO and annular modes have a "red spectrum" as characterized by an AR-1 (autoregressive process of first order) or, as it is also known, an Ornstein-Uhlenbeck process.

There is evidence, however, that the zonal index persists longer than would be expected from this simple reddening argument due to interactions between the eddies and the large scale flow. Lorenz and Hartmann (2001) developed a technique to estimate the linear damping timescale of the zonal index absent any interaction between the eddies and large scale flow. Their analyses suggest that the observed e-folding timescale of the zonal index in the Southern Hemisphere ($\approx$ 13 days) is a little longer than the natural damping timescale of anomalies (8.9 days), providing some evidence of a feedback between the eddies and the

large scale flow. They propose a feedback based on changes in the index of refraction associated with shifts in the extratropical jet, which allow the jet to shape the higher frequency eddies. Independently, Kidson and Watterson (1999) and Watterson (2002) consider the behavior of the zonal index in the Southern Hemisphere of an atmospheric GCM coupled to a mixed layer ocean. While they found that a simple AR-1 model could replicate the basic behavior of the zonal index, a positive feedback between the high frequency eddies and the index was necessary to explain the correlation of the index at long lags.

Mechanisms for enhanced persistence have been discussed previously in other forms by several authors, (e.g. Branstator 1992, 1995; Feldstein and Lee 1998; Robinson 1994, 1996, 2006). It is reasonably well established that the zonal index and NAO are forced by eddy momentum fluxes. The potential for low frequency anomalies, which are largely barotropic, to in turn influence the baroclinic eddies, thereby completing a feedback loop, has been harder to establish. Branstator (1995) used a linear model to predict the synoptic response to the intraseasonal anomalies. The resulting change in the storm track was such as to reinforce the anomaly. Robinson (2006) argues that the eddies increase the baroclinicity in the jet core relative to the flanks, so helping to maintain the existence of the jet. This self-maintenance mechanism reinforces the jet at the latitude of peak winds, and so could extend persistence of jet anomalies as well.

In this paper, we use a dry primitive equation model of the atmosphere to focus on the interactions between eddies and the large scale flow. It has been demonstrated that atmosphere-only models can well capture the essential dynamics of both the NAO and annular modes (Limpasuvan and Hartmann 2000; Cash et al. 2002). Simplifications to the forcing of the our GCM provide a realistic climatology governed by a few well-defined parameters, so that the internal damping timescales are known. The simplifications also

allow us to explore the variability around a wide range of climatologies. We demonstrate that the timescale on which the jet varies is distinct from any of the prescribed timescales in the model, providing evidence of eddy-mean flow feedback. The feedback, however, is extremely sensitive to zonal asymmetries in the large scale forcing. The destruction of the feedback appears to be related to zonal asymmetry in the eddy forcing, and is currently being investigated by the authors in a continuation of this study.

Our experiments and analysis procedures are discussed in Section 2. We then survey the model over parameter space in Section 3. We find that a number of aspects of the model's behavior respond similarly to changes in three parameters — the equilibrium equator-to-pole temperature gradient and the temperature and momentum damping coefficients. Absent zonal asymmetry in the forcing, the timescale of the model's annular mode is quite sensitive to the parameters. This sensitivity, however, is largely eliminated in the presence of zonally asymmetric forcing. Section 4 presents a diagnostic of the model's zonal index to establish a more intuitive understanding of the physical pattern. A mechanism for a feedback between eddies and the mean flow is described in Section 5. Section 6 summarizes our results and conclusions.

2. Experimental Design

We use a spectral, dry primitive equation model with 20 evenly spaced $\sigma = p/p_s$ vertical levels, where p_s is the surface pressure. The model forcing is idealized, as described in Held and Suarez (1994) (hereafter denoted HS), with a steady Newtonian relaxation to a prescribed temperature field. Thus, the thermodynamic equation is

$$\frac{DT}{Dt} - \frac{\kappa T \omega}{p} = -k_a(T - T_{eq}), \tag{2.1}$$

where $\kappa = R/c_p$, R is the ideal gas constant, and c_p the specific heat of dry air. In the standard HS scheme, the damping, k_a, is almost everywhere set to 40^{-1} day^{-1}, the exception being in the low level tropics, where it is increased to 4^{-1} day^{-1} at the surface to establish a more realistic Hadley Circulation. The equilibrium profile T_{eq} is determined by a small number of parameters, the most significant for our purposes being the equator-to-pole temperature difference, ΔT_{eq}. Momentum is removed from the model near the surface by a Rayleigh drag of strength k_f, which decays linearly in σ to the 0.7 level, where it vanishes. A ∇^8 damping is included to remove enstrophy at small scales, the coefficient set so that damping time on the smallest resolved scale is $1/10$ of a day. For reference, the key parameters and their default values in the control run are listed in Table 1.

We report on eight sets of experiments, as outlined in Table 2. With the exception of set II, all simulations were completed with triangular truncation at total wavenumber 42, or "T42." In exploring the model behavior, we recognized a troubling sensitivity to vertical resolution. At T42 horizontal resolution, the model's zonal index becomes very persistent when the spacing of vertical levels is made particularly fine near the upper boundary of the atmosphere, as discussed in the Appendix. Given this deficiency, we focus on trends in the timescales of variability as opposed to the absolute numbers themselves. Care was taken to verify key trends at resolution T63, where the behavior is less sensitive to vertical resolution.

Experiment sets I through IV explore the sensitivity of the variability to model parameters. The forcing is the same in both hemispheres and independent of longitude, as in the standard HS scheme. Since the two hemispheres were statistically independent, we sampled from both to double our data set. In experiment III, where k_a is varied, the strong damping in the low level tropics is not changed to minimize change to the tropical circu-

lation. The sensitivity of the variability to zonally asymmetric forcing is determined in experiments V through VIII. Asymmetry is introduced through large scale perturbations to the equilibrium temperature profile that approximate land-sea contrast and idealized topography of comparable scale to the Rocky Mountains. A single zonally localized storm track is established, providing a rough approximation to the wintertime Northern Hemisphere, and producing NAO-like variability. The details of the perturbations are described in the Appendix, and their influence on the spatial structure of synoptic and intraseasonal variability is the focus of current research. Perturbations were placed only in the model's Northern Hemisphere.

As is conventional, we define the zonal index as the principal component associated with the first EOF of the daily zonally averaged zonal winds on the $\sigma = 0.975$ level, the closest level to the surface. The bias due the decrease in separation of grid points at high latitudes in EOF computations was corrected by weighting fields with a factor of $\cos^{1/2}\theta$ (North et al. 1982). The annular mode is defined as the first EOF of the 10 day averaged SLP, and the annular mode index is the time series of this pattern, found by projecting the daily SLP field onto the EOF. This first EOF (not shown) becomes NAO-like in structure in the zonally asymmetric runs. The correlation coefficients between the zonal index and annular mode index are greater than 0.9, even in simulations with significant zonal asymmetry. Thus the model's zonal index, annular mode, and "NAO" (in asymmetric runs) describe much the same pattern of variability. The timescale of the zonal index/annular mode was quantified by the best exponential fit to the autocorrelation function of the index for all lags until the autocorrelation dropped below 0.3. The autocorrelation functions were not purely exponential, but tended to exhibit steeper decay on short lags with a broad shoulder at longer lags. As they are roughly self-similar, however, the e-folding timescale

provides a good comparative measure.

3. Results

The mean circulation and variability respond in a quite similar fashion to changes in the equilibrium temperature gradient ΔT_{eq}, thermal damping rate, k_a, or momentum damping rate k_f. Figure 1 highlights the near equivalence of the climatological response. The top panels, (a) and (b) show the time and zonal mean zonal wind for two simulations with differing values of ΔT_{eq}. With a doubling of the temperature gradient, the extratropical jet shifts poleward by approximately 9° and the time average surface winds double. As seen in panel (c), the difference in the mean winds between these two simulations, the increase in ΔT_{eq} leads to a mild strengthening of the subtropical jet near 20°, a more substantial increase in the extratropical jet near 50°, and a slight weakening of the winds in between. Panels (d) and (e) illustrate the difference between simulations when the values of k_a and k_f are varied, respectively. The response to all three parameters is similar both in *structure* and *amplitude*: the same fractional change in ΔT_{eq}, k_a, or k_f leads to similar amplitude response. The sign of the response, however, has reversed for the surface friction; the poleward shift of the jet and increase in the surface westerlies observed with an increase in the thermal forcing occurs with a decrease in k_f.

Perhaps most striking is the fact that the parameters have a similar effect on the timescale of intraseasonal variability. Figure 2 summarizes the results of the 14 simulations in experiment sets I through IV, showing the e-folding timescale of the zonal index as a function of the three parameters. In panel (a), we focus on the similarity in the sensitivity to ΔT_{eq} and k_a. The solid and dot-dashed black curves show the timescale as a function of ΔT_{eq} for two different resolutions, and correspond with the units on the lower x-axis. The sensitivity to

variations in k_a is shown by the dashed gray curve, with values of the coefficient specified on the upper x-axis. Increasing ΔT_{eq} or k_a leads to a drop in the timescale of variability. ΔT_{eq} was varied over a wider range from the control value, 60 K, in experiment I. The sensitivity appears to saturate for high values above 80 K, and break down when the forcing becomes too weak, at 30 K. At T63 resolution, the model is significantly less sensitive to ΔT_{eq}, but the sensitivity is still of the same sign. Panel (b) compares the sensitivity to ΔT_{eq} with that to k_f; the sensitivity to k_f is similar, but again of opposite sign. In summary, the timescale of the zonal index is reduced by (1) an increase of the equilibrium temperature gradient, (2) a strengthening of the thermal damping, or (3) a weakening of the momentum damping.

Given the similar sensitivity of the model to each of the three parameters, we use only one, the equilibrium temperature gradient, to probe the sensitivity of intraseasonal variability to zonally asymmetric forcing. ΔT_{eq} is perhaps the most physical parameter, and can be linked to changes in forcing during the seasonal cycle, or changes to the climate, e.g. a reduction of the ice-albedo effect due to global warming may reduce the equator-to-pole temperature contrast. Figure 3 summarizes the results from experiment sets I and V through VIII. For each experiment we compare the e-folding timescale of variability in three simulations in which the equilibrium temperature gradient is varied from 40 to 60 to 80 K. The black curve on top illustrates the dramatic sensitivity of the intraseasonal variability to ΔT_{eq} absent any zonal asymmetries, as seen from Figure 2. With increasing zonally asymmetric forcing, however, this sensitivity is weakened, and finally eliminated, as observed by the flattening of the sensitivity profiles.

When the equilibrium temperature gradient is varied from 40 to 80 K in the zonally symmetric model (experiment set I), the e-folding timescale of the annular mode decreases

over fourfold, from 93 to 21 days. When the gradient is varied to the same extent in simulation set VIII, where we have introduced both topography and a diabatic heating anomaly to model land-sea contrast, the e-folding timescales are substantially shorter and nearly independent of the equilibrium temperature gradient, varying from 10–13 days. This is consistent with the timescale observed of the northern annular mode. The timescale of the southern annular mode, as analyzed in a more sophisticated GCM by Watterson (2007), exhibits a 50% variation within the seasonal cycle. This suggests that the sensitivity of the e-folding timescale to ΔT_{eq} in experiments VI and VII is not unreasonable. These are perhaps the most relevant simulations to the Southern Hemisphere, which does contain substantial large scale asymmetry, such as the Andes Mountains.

To compare timescales of intraseasonal and synoptic variability, we compute an eddy turnover timescale $L/K^{1/2}$. K is the eddy kinetic energy, averaged over the depth of the troposphere $\pm 15^\circ$ from the jet core. L is an eddy length scale determined from the zonal Fourier spectrum of the meridional velocity, v, at the latitude and height of the peak eddy kinetic energy, θ_{Kmax} and p_{Kmax}:

$$L = 2\pi r_0 \cos(\theta_{Kmax})/k_{ave} \tag{3.1}$$

where r_0 is the radius of the earth and the average wavenumber k_{ave} was computed by,

$$k_{ave} = \sum_{k=1}^{64} k\,[\tilde{v}_k^2] \Big/ \sum_{k=1}^{64} [\tilde{v}_k^2] \tag{3.2}$$

where $\tilde{v}_k(t)$ is the k^{th} Fourier coefficient of $v(t,\phi,\theta_{Kmax},p_{Kmax})$, and brackets refer to the time mean. The eddy turnover timescale varies only slightly with parameters. In simulation sets I and II, K increases linearly with the equilibrium temperature gradient, so that the eddy turnover timescale varies with $\Delta T_{eq}^{-1/2}$, as shown in Figure 4. The eddy kinetic energy did not change as much in experiments III and IV. There was a slight decrease in K with

a decrease in the thermal or momentum damping, k_a or k_f, leading to rise in the eddy turnover time in both cases. The timescale of the zonal index increases with decreasing k_a, but decreases when k_f is reduced. Hence there is not a consistent relationship between the timescale of individual eddies and the jet as a whole. In addition, the relationship between the parameters and eddy statistics is not affected when large scale asymmetries are introduced despite the dramatic changes in the jet variability.

4. The Zonal Structure of the Zonal Index and Annular Mode

What sets the timescale at which the extratropical jet varies in our model? In the zonally symmetric simulations, the parameters ΔT_{eq}, k_a, k_f can be viewed as knobs that allow one to vary timescales in the model. Parameters k_a and k_f set damping timescales, while ΔT_{eq} largely controls the eddy turnover timescale. The similar sensitivity of the timescale of the zonal index to all three knobs thus allows one to change it independently of any two of the three internal timescales. This suggests that the zonal index varies on a distinct timescale and is not simply determined by any one of the model's internal timescales. When zonal asymmetries are included, the timescale of intraseasonal variability decreases, and becomes largely independent of one of the knobs, the equilibrium temperature gradient. The zonally averaged eddy kinetic energy and other eddy statistics, however, remain as sensitive to the gradient as they were in the zonally symmetric simulations. The chief difference is in the zonal structure of the eddy statistics, since eddies have become organized into a zonally localized storm track.

To seek out common features in simulations with the same degree of persistence, we

develop a diagnostic of the annular mode as a function of both *time* and *longitude* (motivated in part by Feldstein (2000a), who considered the contribution of the zonal wind at each longitude to the zonal index to assess the coherence of the flow). We compute the first EOF, $Z(\theta)$, of the daily zonally averaged surface zonal wind, u_s, and the associated principal component, $Z_I(t)$, which is the model's zonal index. The EOF patterns are shown in relation to the mean surface winds for two different simulations in Figure 5 The EOFs shift with the jet, remaining out of phase with the mean surface winds and so always characterizing a shift in the latitude of the jet. We then project the flow at all times and longitudes onto $Z(\theta)$, so generating a local dipole index that is a function of both time and longitude; that is, we compute

$$D_I(t,\lambda) = \alpha \int_0^{\pi/2} Z(\theta) u_s^*(t,\theta,\lambda)\cos(\theta) d\theta \tag{4.1}$$

where * refers to deviations from the time mean and the cosine accounts for the latitude bias. The normalization constant α is chosen so that the zonal average of the dipole index has unit variance. Thus, $\int_0^{2\pi} D_I(t,\lambda)d\lambda = Z_I(t)$, namely the original zonal index. In our model, the annular mode index captures the same variability as the zonal index; the EOFs associated with the two indices are in geostrophic balance and both characterize a meridional shift in the jet. The correlation between the two indices is above 0.9 in all simulations. Hence $D_I(t,\lambda)$ also allows us to see the zonal structure of the annular mode.

Figure 6 illustrates the evolution of the local dipole index for two simulations from experiment I with equilibrium temperature gradient $\Delta T_{eq} = 40$ and 80 K, respectively. The curves on the right of each map show the evolution of the zonal index. Both diagrams are dominated by short lived, eastward propagating features of limited zonal scale, perhaps wavenumber 5 or 6. (Kushner and Lee (2006) found similar eastward propagating features.) Even in this short time slice, one can see greater persistence of the zonally averaged

signal in the simulation with $\Delta T_{eq} = 40$ than in the simulation with $\Delta T_{eq} = 80$, but locally the slowly evolving signal is masked by the shorter lived features. The amplitude of D_I anomalies is larger in the $\Delta T_{eq} = 80$ simulation. This is related to the scaling of the index, which is chosen so that the zonal average of the local index gives the traditional zonal index. Weaker coherence in the zonal flow will then lead to a higher variance of the dipole index.

We next compute the autocorrelation of the dipole index as a function of time lag and longitude. Given the statistical zonal symmetry of these simulations, the lag-longitude autocorrelation can be averaged over all longitudes to improve the statistics, producing one overall map. The maps in Figures 7 and 9 are arbitrarily based from a reference longitude at 180°, but characterize the flow at all longitudes. Figure 7 focuses on the dominant feature of the lag-longitude correlation map, which captures the scale and slow eastward propagation of the local structures in Figure 6. The features extend over a range of 50-60° and persist for 2-4 days in both simulations. They propagate eastward at approximately 7° a day (8 ms^{-1} at the latitude of the jet maximum) in the simulation with $\Delta T_{eq} = 40$ and 16° a day (14 ms^{-1}) in the simulation with $\Delta T_{eq} = 80$. Such spatial and temporal scales suggest that these features are the projection of a single eddy, or single wave breaking event, onto the meridional structure of the dipole index, as depicted in the diagram in Figure 8. Indeed, composites of such features in Kushner and Lee (2006) had a baroclinic structure in the vertical, suggesting a composite of baroclinic eddies that have projected onto the zonal index.

Figure 9 illustrates the same lag-longitude autocorrelation maps, but the grayscale has been saturated at correlation 0.4 and the range widened. A wavetrain about the reference point provides further evidence that synoptic eddies are projecting onto the zonal index (or

annular mode) pattern. The wave packet in the simulation with $\Delta T_{eq} = 40$ is characterized by wavenumber 6 and propagates 23° a day. When $\Delta T_{eq} = 80$, the packet is of wavenumber 5, and propagates 38° a day. (The jet is located further poleward here, so the length scale has not increased significantly.) Based on the latitude of the jet maximum, the respective group velocities are 24 and 33 ms^{-1}, respectively, consistent with the jet speeds in the two simulations, 27 and 37 ms^{-1}.

The wavetrain in the simulation with $\Delta T_{eq} = 40$, however, is superimposed on a higher background correlation than with $\Delta T_{eq} = 80$. At lags beyond 10 days the correlation becomes independent of longitude, indicating zonally coherent behavior at longer timescales. We can quantify the significance of the hemispheric coherence at zero lag by estimating the strength of the uniform correlation beneath the projection of the individual eddies and wave trains on the local index. When $\Delta T_{eq} = 80$, the zonally uniform motion is at best 0.15 correlated with the local flow, while in the persistent simulation with $\Delta T_{eq} = 40$, this signal is more than doubled in strength. This zonally coherent signal represents a truly hemispheric pattern of variability, not necessarily a mode in the linear sense, but a slow vacillation of the entire eddy driven jet with a timescale of its own.

This analysis suggests why it may be difficult to see an annular pattern in a synoptic map, as also highlighted by Figure 7 of Cash et al. (2002). The zonal index is generally dominated by local features seen in the Hövmöller diagrams in Figure 6. In the simulation with $\Delta T_{eq} = 80$, the zonally uniform signal is dominated by local events to the extent that it makes little difference to the zonal index. The annular mode in this case is largely a statistical feature, as suggested by the minimal model in Gerber and Vallis (2005). In the simulation with $\Delta T_{eq} = 40$, rather, there is a significant hemispheric signal that is masked, to some extent, by local events riding on top the uniform movement of the jet. Synoptic

variability hides the hemispheric signal unless it is filtered in space or time.

In simulations with zonally asymmetric forcing, analysis of the local dipole index suggests that the dynamics have changed qualitatively from the zonally symmetric case, consistent with the change in persistence. Consider a simulation from experiment VIII, where both land-sea contrast and topography have been included, with the standard value of $\Delta T_{eq} = 60$. Lag-longitude autocorrelation maps of the local dipole index are shown for two longitudes in Figure 10. In panel (a), the base longitude is in the peak baroclinic zone at the entrance to the storm track. Even with the grayscale saturated at correlation 0.45, the map is dominated by the local phase behavior, which indicates features propagating eastward 16° per day. Excepting the region immediately downstream the base point, the correlation with other longitudes is below 0.05 for all lags. The base longitude chosen for panel (b) is located in the region of peak intraseasonal variability, as characterized by the first EOF of sea level pressure, but this pattern is characteristic of all latitudes outside the storm track. The map indicates slower phase propagation and more extended correlations in time and space. There is a distinct drop in the autocorrelation, however, with points in the baroclinic region between 80 and 120°. This barrier is observed for all base points chosen outside the storm track.

Similar structure is observed in other simulations with storm tracks. Zonal asymmetries, particularly topography, inhibits the uniform correlation observed in zonally symmetric simulations. Even when the large scale forcing is favorable to strong persistence, with $\Delta T_{eq} = 40$, the storm track forms a barrier to zonally coherent motions. The addition of zonal asymmetries thus has the same effect as increasing the temperature gradient in the zonally uniform simulations. In all these simulations, the zonal index and annular mode do not reflect coherent movement of the jet. Rather, localized eddies, wave packets, and wave

breaking events are driving the zonally averaged flow about.

It is only in the more persistent simulations, with weak ΔT_{eq} or k_a, or with strong surface friction, k_f, that the zonal index and annular mode describe a truly hemispheric variation. Individual eddies are less significant in determining shifts of the jet in these simulations. These uniform shifts of the extratropical jet may allow for, or rather result from a feedback between the eddies and the zonal mean flow.

5. Interaction between Eddies and the Large Scale Flow

In this section we suggest a mechanism by which synoptic eddies interact with the mean flow to reinforce the extratropical jet at the latitude of maximum winds. This causes the zonal mean jet to become "sticky," tending to meander slowly on a distinct timescale set by the strength of the eddy-mean flow interactions. We argue that synoptic eddies more efficiently reduce the shear at latitudes at which the upper level flow is weak. Hence the eddies will increase the baroclinicity of the flow in the jet core *relative* to the baroclinicity on the flanks of the jet. While this property helps sharpen and reinforce the jet, as discussed in the context of a two layer model by Robinson (2006), it also extends the persistence of jet anomalies.

The zonal index and annular mode anomalies are primarily barotropic, or at least equivalent barotropic, limiting their direct influence on the growth of baroclinic eddies themselves. [Barotropic shear can effect eddy growth, as (James 1987) and Nakamura (1993) discussed. These effects will be discussed further below.] They indirectly affect the eddies, however, by changing the position of the critical latitudes of the flow, which influence wave breaking. Linear theory suggests that irreversible mixing — the damping of wave activity — occurs at critical layers where the phase speed of the wave, c, equals that of the mean

flow $\overline{u}$. Particle displacements, η, scale as $\psi/(\overline{u}-c)$, where ψ is the streamfunction perturbation, so that displacements will grow unbounded even for infinitesimal perturbations, leading to nonlinearity as the wave approaches the critical latitude Randel and Held (1991).

As a thought experiment, consider a barotropic jet perturbation within a wider baroclinic region. The barotropic jet must be maintained against friction by an upgradient momentum flux. A divergence of wave activity generated by eddies growing within jet provides the momentum source (Edmon et al. 1980). Growth of eddies centered on the flanks of the jet yields a source of wave activity outside the jet core, and divergence of this flux will shift the latitude of the barotropic jet, thus changing the state of the zonal index or annular mode (Vallis et al. 2004). We contrast these two cases, eddy generation centered about the jet core versus on the flank, with a focus on their influence on the baroclinicity of the flow to determine how they feedback on future eddy generation.

Panels (a) through (c) of Figure 11 schematically illustrate the influence of eddies generated in the jet core on the mean flow. Panel (a) shows the effect of heat fluxes generated by the growing eddy. Poleward heat fluxes are associated with the vertical propagation of wave activity (the Eliassen-Palm flux), which reduces the shear, drawing momentum from the upper to lower levels.[1] Momentum is not extracted from the flow, however, until the wave activity dissipates. The zonal average flow $\overline{u}$ is strongest where the barotropic circulation augments the upper level flow, allowing wave activity to propagate meridionally until it nears critical latitudes on the flanks of the jet. The resulting divergence of wave activity leads to an upgradient transfer of momentum at upper levels, panel (b). The net effect of the eddy life cycle, panel (c), is still a weakening of the upper flow in the jet core, but the

[1]Eddy heat fluxes reduce the shear by weakening the temperature gradient. In the Transformed Eulerian Mean framework this is characterized by the vertical propagation of wave activity. In the Eulerian framework, the mean meridional circulation brings momentum to the surface.

weakening has been spread to the flanks of the jet as well. Thus the tendency of the eddy heat transport to reduce the baroclinicity has been partially offset by momentum transport in upper levels.

Now contrast this with an eddy which grows on either flank of the jet, as illustrated in panel (d). In this case heat fluxes associated with eddy growth also lead to vertical propagation of E-P fluxes. But the weaker zonal velocity $\overline{u}$ at upper levels limits meridional propagation; weaker flow supports fewer waves, as only waves with phase speed less than $\overline{u}$ can exist. The waves are nearer their critical latitude, and damped more quickly. Thus the tendency of the heat fluxes to reduce the shear is not offset by a convergence of momentum. The initial eddy will begin to shift the barotropic circulation, but there is also a substantial change in the shear, making it less favorable for a second eddy to form at this latitude. This negative feedback limits the ability of the jet to move, thereby reinforcing the current position of the jet.

The barotropic jet associated with the zonal index and annular modes thus helps maintain the baroclinicity in the jet core, irrespective of the current latitude of the jet. We use maintain in a relative sense, however, as the eddies universally reduce the baroclinicity. The key is that *the eddies are more efficient at reducing the baroclinicity if they form on the flanks of the jet.* This suggests that the mechanism is perhaps best viewed as a *negative* feedback on movement of the jet. In terms of the persistence of the jet anomalies, however, a negative feedback on movement is the same as a positive feedback on staying.

Spherical geometry requires a small correction. Eddy growth is determined by the baroclinicity, which peak poleward of the region of maximum shear, and so poleward of the upper level jet maximum. The offset arises primarily from the Coriolis parameter in the

thermal wind equation,

$$u_z = \frac{1}{f} d\theta / dy. \tag{5.1}$$

There is thus a factor of $\sin^{-1}\theta$ shifting the maximum shear equatorward of the region of maximum temperature gradient. As eddy growth is preferred on the poleward flank of the maximum upper level winds, equatorward propagation will be favored, and momentum is extracted from the subtropics preferentially over the polar region (Simmons and Hoskins 1978). This bias may lead to poleward propagation of zonal wind anomalies, as discussed by Feldstein (1998). If such propagation dominates, it may set the timescale of the zonal index.

We find evidence of the above mechanism in our model by analyzing the Eliassen-Palm fluxes (e.g., Edmon et al. 1980). The flux takes the form

$$\boldsymbol{F} = \{\overline{-u'v'}, f\frac{\overline{v'\theta'}}{\overline{\theta}_p}\} \tag{5.2}$$

where an overbar denotes the zonal average and primes deviations there from. Meridional divergence of the first term captures the direct momentum forcing by the eddies, while vertical divergence of the latter term characterizes the impact of eddy heat fluxes on the zonal momentum. We use the 2-10 band pass filtered E-P fluxes to focus on the behavior of synoptic eddies. By averaging the net divergence of the flux over two halves of the atmosphere, above and below 500 hPa, we can simplify analysis of our GCM to that of a 2-layer model and make a connection with the analysis of Robinson (2006).

We first consider the role of the eddies in the neutral state, the average over all times when $|Z_I(t)| < 1$. The contribution of the eddy momentum and heat fluxes, divergence of the first and second terms in (5.2), to the zonal momentum forcing budget in the control simulation are shown in Figure 12. Focus on the upper curves, which show the impact of the eddies on the flow above 500 hPa. The dot-dashed contours show acceleration of

the mean flow due to eddy heat transport, negative (easterly) for all latitudes in the upper half of the atmosphere. The dashed curve, the impact of eddy momentum fluxes, indicates transport of momentum into the jet core. While this is not enough to offset the momentum lost to the lower layers, it does produce a relative minimum in the net torque, shown by the solid curves. This minimum is the self-maintaining, or self-sharpening property of the eddy fluxes described by Robinson (2006): the eddies, on average, tend to reduce the shear in the jet core slightly less than on the flanks. The key lies in the fact that easterly torque due to heat fluxes is broader than the westerly torque due to momentum fluxes. Sharpening of the baroclinicity is also dependent on surface friction to cancel the westerly torque in the lower layer. Otherwise the shear is reduced by an increase in the surface winds.

Composites associated with positive and negative zonal index events for the standard HS control run are shown in Figure 13. The dashed curves on the top show the easterly acceleration of the zonal average zonal wind by 2-10 band pass eddy fluxes in the upper half of the atmosphere. The minimum in the easterly acceleration on the upper level flow remains coincident with the zonal mean jet, shown by the solid curve: eddies reinforce the jet anomalies in both cases. The dot-dashed curves show the westerly acceleration of the lower half of the model's atmosphere. This is almost entirely due to heat fluxes; the poleward offset from the jet maximum is consistent with the discussion of (5.1). It can also be seen that the mechanism is best viewed as a negative feedback on movement of the jet. The eddies are everywhere reducing the baroclinicity; they are just more effective on the flanks of the jet than in the core.

6. Summary and Conclusions

Using a simplified GCM, we have explored the way in which the intraseasonal variability depends on various parameters in order to understand the potential for interaction between synoptic eddies and the large scale flow. Power on 10–100 day timescales was found in broad meridional dipole patterns similar in structure to the observed zonal index and annular modes. Absent zonally asymmetric forcing, the timescale of the model's zonal index was found to be sensitive to three model parameters: the equilibrium equator-to-pole temperature gradient, ΔT_{eq}, the thermal damping, k_a, and the momentum damping, k_f. The first parameter regulates the eddy heat transport of the model, and thus the eddy kinetic energy, while the latter two set internal damping timescales. A decrease in ΔT_{eq} or k_a, or an increase in k_f, led to an equatorward shift in the mean jet and increase in the e-folding timescale of the zonal index. Since there exist three independent parameters that can be used change the timescale of the index, we conclude that it is distinct from any one of them individually; rather, the index time scale is being generated by an internal dynamical process, an eddy-mean flow interaction, although the index timescale must presumably depend, and in some complicated way, on a combination of the parameter timescales

The timescales of the model changed quite dramatically when topography and large scale thermal forcing were introduced to create a zonally localized storm track. Zonal asymmetries reduced the timescale of the intraseasonal variability and its sensitivity to model parameters. In the most realistic simulations, the timescale in fact became largely independent of the model parameters and quite consistent with timescales from observations.

We developed a simple diagnostic, a local dipole index, $D_I(t,\lambda)$, to explore the local, zonal structure of the zonal index and annular modes. The aim was seek out common

features from simulations with the same degree of persistence and come to a more intuitive understanding on the nature of the zonal index in our model. On shorter timescales, the zonal index does *not* reflect zonally coherent motion. Locally, the dynamics are dominated by the projection of synoptic features onto the zonal index dipole. On longer timescales, however, we found that there is a true annular signal in the simulations with weak thermal forcing or strong surface friction — those simulations with more persistent zonal index behavior. This indicates the presence of a slow, coherent shift of the extratropical jet. Whereas the annular mode in these simulations is not a mode in the linear sense, it does have physical significance in that it characterizes a hemispheric shift in the extratropical jet where strong nonlocal interactions between the mean flow and eddies may be active. As seen in Figure 9, after 10–15 days the correlation of the local dipole projection becomes largely *independent* of longitude. This weaker, zonally coherent signal is masked, to some extent by synoptic variability that dominates the projection at shorter timescales.

In simulations with stronger thermal forcing, weaker surface drag, or zonally asymmetric forcing, where the zonal index was not as persistent, there was very little underlying zonally-coherent behavior. The zonal index (and annular mode) are still the dominant patterns of low frequency variability in these simulations as determined by an EOF analysis, but their dominance is better understood from the statistical perspective of Gerber and Vallis (2005). Most of the power comes from smaller scale, local projections of individual eddies and wave breaking events, not a hemispherically coherent movement of the jet. Zonally asymmetric forcing, topography in particular, creates a barrier to zonal coherence. In the storm track the zonal index is dominated by swiftly moving synoptic eddies. The flow does become more zonal and persistent outside the storm track, but the zonally coherent signal is completely lost.

To explain the enhanced persistence in zonally symmetric simulations, we formulated a mechanism for coupling between eddies and the barotropic flow, inspired in part by the self-maintaining jet theory of Robinson (2006). We argue that the barotropic flow shields the baroclinicity of the jet, making eddies less efficient at reducing the shear in regions where the upper level flow is strong. This causes the zonal mean jet to become "sticky," tending to meander slowly on a distinct timescale set by the strength of the eddy-mean flow interactions. The mechanism depends on the balance between eddy heat transport in the lower troposphere (the production of wave activity) with eddy momentum transport above (the propagation and dissipation of wave activity). The surface westerlies and the barotropic jet may be considered to be maintained against surface friction by the westerly torque associated with the divergence of wave activity near the surface. The jet is thus tied to the latitude of peak eddy generation; a shift in the eddies leads to a shift in the jet on the relatively short timescale of the surface drag. If the eddies evolved independently of the mean flow, one would expect jet variations to be characterized by a red noise process in time, shouldering on a timescale set by the frictional drag and eddy processes that communicate surface friction to the upper level flow. The barotropic flow, however, can influence eddy generation by shaping the meridional propagation and dissipation of waves in the upper atmosphere, making a feedback loop possible.

Linear theory suggests that waves are damped near critical latitudes, where the phase speed of the wave, c equals that of the flow, $\overline{u}$. As waves approach the critical latitude, large particle displacements lead to wave breaking and irreversible mixing. The barotropic flow in the jet core increases the zonal velocity, permitting the jet to support more wave activity and enabling waves to propagate farther before they near critical latitudes. Momentum is transported in the opposite direction of the wave activity flux, and so tends to converge into

regions of stronger flow. This torque partially offsets the tendency of eddies generated in the jet core to reduce the shear. Wave activity generated by eddies on the flanks of the jet, rather, will be damped more closely to the latitude at which it was generated; waves are simply closer to their critical latitudes. Hence eddies can more efficiently reduce the shear where the upper level flow is weaker, and there is a negative feedback against sustained eddy growth on the flanks of the jet. This acts to retard motion of the jet, inhibiting eddies from shifting the barotropic circulation.

Surface friction plays a role in the feedback, in a fashion similar to that discussed in a 2-layer model by Robinson (1996). Eddy heat fluxes produce a large westerly acceleration of the lower layers, so acting to reduce the shear, as shown in Figure 12. By comparison, the feedback mechanism is evidenced in the shallow minimum in the easterly acceleration of the upper level flow. If surface friction does not damp the westerly torque on the lower layers, the shear will be reduced by the increase in the winds at the surface, and the small minimum aloft will be rather inconsequential. In other words, without strong surface momentum damping, the shear is determined more by the low level circulation. Momentum redistribution in the upper levels will not be able to maintain the shear and the barotropic circulation is no longer able to shape the stirring. The sensitivity of the timescale of the zonal index to the momentum damping, k_f, may follow from these arguments. The jet becomes more persistent when k_f is increased, and the westerly acceleration of the flow by the heat fluxes is more strongly damped.

The timescale of jet variation, however, is equally sensitive to the other parameters, the equilibrium temperature gradient, ΔT_{eq}, and the thermal damping, k_a. These parameters control the thermal restoring force on the flow, and are not easily connected to changes in the surface friction. With all three parameters, weaker persistence is consistently associated

with a stronger barotropic circulation (see Figure 1). As discussed by James (1987), and established in a more theoretical framework by Nakamura (1993), barotropic shear can directly influence eddy growth. These influences may compete with the indirect impact of the barotropic flow discussed in Section 5 and limit the eddy-mean flow interaction when there is strong barotropic shear. This may link the stronger barotropic jet to the weaker persistence, in which case the sensitivity to all parameters can be related to their impact on the mean flow, and remains an open question for further research.

The dramatic breakdown of the jet variation timescale in simulations with topographic and large scale thermal forcing is associated with the loss of the zonally coherent motion, as suggested by the analysis in Section 4. A pathway for the breakdown of the eddy-zonal mean feedback in the presence of zonally asymmetric forcing is the subject of current research. There is evidence that the key lies in the separation of eddy growth and decay in the storm track.

ACKNOWLEDGMENTS We thank Ian Watterson and two anonymous reviewers for insightful comments and suggestions on an earlier version of the manuscript. This work is partially supported by the NSF, ATM division. EPG also thanks the Fannie and John Hertz Foundation for support.

Appendix

a. Resolution Sensitivities

At T42 resolution, the timescale of the zonal index is sensitive to vertical resolution in the upper atmosphere. This sensitivity can be found either by adding more levels evenly through the atmosphere, or by keeping the same number of levels and adjusting the spacing

as to increase resolution in the upper atmosphere at the expense of the lower and mid troposphere. This increase in timescale (which can be dramatic) is associated with the same shift in the mean state observed in the parameter sweep experiments described in Section 3.

It was discovered, however, that this increase in timescale is not robust to changes in horizontal resolution. At T63, the model ceases to be sensitive to the vertical resolution; the timescales of simulations with both low and high vertical resolution at the upper boundary do not change significantly. Experiments with the model at T63 and T85 resolution indicate that the model's behavior at T42 is more robust with coarser vertical resolution than with finer resolution. This is to say, increasing the vertical resolution at T42 appears to introduce a pathology into the model. Mindful of this weakness of the model, we verified key trends at higher resolution, where the model behavior is more robust. A more thorough discussion of the resolution issue can also be found in Section 5.4 of Gerber (2005).

b. Zonal Asymmetries

We experimented with mountains of varying shape and height and found the results to be relatively robust provided the orography was positioned as to block the extratropical jet. In the simulations described here, we use a Gaussian ridge of variable height, as described in Table 2, comparable in horizontal scale to the Rocky or Andes Mountains. The half-width of the ridge in longitude is 12.5 degrees. The ridge is 40° long in latitude and centered at 40° N. It tapers off with a half width of 12.5° at either end, so that it does not extend into the Southern Hemisphere.

A thermal perturbation[2] was introduced to approximate the affect of land-sea contrast

[2]Note that in the implementation of the HS forcing, T_{eq} is not allowed to drop below 200 K, the temper-

between a cold continent and warm ocean in the winter hemisphere. We experimented with several variations, settling with a simple perturbation δT_{eq} to the zonally uniform profile that produced the desired zonal asymmetry in the synoptic variability,

$$\delta T_{eq}(\lambda,\theta,\sigma) = k f_\lambda(\lambda) f_\theta(\theta) f_\sigma(\sigma). \tag{A.1}$$

where λ, θ, and $\sigma = p/p_s$ are the longitudinal, latitudinal, and vertical coordinates, respectively. The horizontal profile was constructed from sine functions,

$$f_\lambda(\lambda) = \begin{cases} 0 & \lambda < \pi/2 \\ \sin(2\sigma) & \pi/2 \le \lambda < 3\pi/2 \\ 0 & \sigma \ge 3\pi/2 \end{cases} \tag{A.2}$$

$$f_\theta(\theta) = \begin{cases} 0 & \theta < 0 \\ \sin(\theta) - \sin(3\theta)/3 & \theta \ge 0 \end{cases} \tag{A.3}$$

In the vertical, the profile is maximum at the surfaces, and decays by a cosine function in σ to zero near the tropopause,

$$f_\sigma(\sigma) = \begin{cases} \cos\left(\pi \frac{1-\sigma}{1.6}\right) & \sigma \ge 0.2 \\ 0 & \sigma < 0.2 \end{cases} \tag{A.4}$$

The resulting heating rates were greater than those observed in the atmosphere, but within range of reasonable. The maximum heat flux into the atmosphere was 400 W/m^2.

ature of the model's stratosphere. We have kept this constraint when applying the perturbation δT_{eq}, thereby truncating the cooling anomaly in upper levels at high latitudes where the temperature would otherwise drop below 200 K.

*References

Barnston, A. G., and R. E. Livezey, 1987. Classification, seasonality, and persistence of low-frequency atmospheric circulation patterns. *Mon. Wea. Rev.*, **115**, 1083–1126.

Branstator, G., 1992. The maintenance of low-frequency anomalies. *J. Atmos. Sci.*, **49**, 1924–1945.

Branstator, G., 1995. Organization of the storm track anomalies by recurring low-frequency circulation anomalies. *J. Atmos. Sci.*, **52**, 207–226.

Cash, B. A., P. Kushner, and G. K. Vallis, 2002. The structure and composition on the annular modes in an aquaplanet General Circulation Model. *J. Atmos. Sci.*, **59**, 3399–3414.

Edmon, H. J., B. J. Hoskins, and M. E. McIntyre, 1980. Eliassen-Palm cross sections for the troposphere. *J. Atmos. Sci.*, **37**, 2600–2616.

Feldstein, S. B., 1998. The growth and decay of low-frequency anomalies in a GCM. *J. Atmos. Sci.*, **55**, 415–428.

Feldstein, S. B., 2000a. Is interannual zonal mean flow variability simply climate noise? *J. Climate*, **13**, 2356–2362.

Feldstein, S. B., 2000b. The timescale, power spectra and climate noise properties of teleconnection patterns. *J. Climate*, **13**, 4430–4440.

Feldstein, S. B., and S. Lee, 1998. Is the atmospheric zonal index driven by an eddy feedback? *J. Atmos. Sci.*, **55**, 3077–3086.

Gerber, E. P., 2005. *A Dynamical and Statistical Understanding of the North Atlantic Oscillation and Annular Modes*. PhD thesis, 252 pp.

Gerber, E. P., and G. K. Vallis, 2005. A stochastic model for the spatial structure of annular patterns of variability and the NAO. *J. Climate*, **18**, 2102–2118.

Held, I. M., and M. J. Suarez, 1994. A proposal for the intercomparison of the dynamical cores of Atmospheric General Circulation Models. *Bull. Am. Meteor. Soc.*, **75**, 1825–1830.

James, I. N., 1987. Suppression of baroclinic instability in horizontally sheared flows. *J. Atmos. Sci.*, **44**, 3710–3720.

Kidson, J. W., and I. G. Watterson, 1999. The structure and predictability of the "High-Latitude Mode in the CSIRO9 general circulation model. *J. Atmos. Sci.*, **56**, 3859–3873.

Kushner, P. J., and G. Lee, 2006. On the zonal structure of the Annular Modes. *J. Climate*, **submitted**.

Limpasuvan, V., and D. L. Hartmann, 2000. Wave-maintained annular modes of climate variability. *J. Climate*, **13**, 4414–4429.

Lorenz, D. J., and D. L. Hartmann, 2001. Eddy-zonal flow feedback in the Southern Hemisphere. *J. Atmos. Sci.*, **58**, 3312–3327.

Nakamura, N., 1993. An illustrative model of instabilities in meridionally and vertically sheared flows. *J. Atmos. Sci.*, **50**, 357–375.

Namias, J., 1950. The Index Cycle and it's role in the general circulation. *J. Meteorology*, **7**, 130–139.

North, G. R., T. L. Bell, R. F. Cahalan, and F. J. Moeng, 1982. Sampling errors in the estimation of Empirical Orthogonal Functions. *Mon. Wea. Rev.*, **110**, 699–706.

Randel, W. J., and I. M. Held, 1991. Phase speed specta of transient eddy fluxes and critical layer absorbtion. *J. Atmos. Sci.*, **48**, 688–697.

Robinson, W. A., 1994. Eddy feedbacks on the zonal index and eddy-zonal flow interactions induced by zonal flow transience. *J. Atmos. Sci.*, **51**, 2553–2562.

Robinson, W. A., 1996. Does eddy feedback sustain variability in the zonal index. *J. Atmos. Sci.*, **53**, 3556–3569.

Robinson, W. A., 2006. On the self-maintenance of midlatitude jets. *J. Atmos. Sci.*, **63**, 2109–2122.

Rossby, C. G., 1939. Relations between variation in the intesity of the zonal circulation and the displacements of the semi-permanent centers of action. *J. Marine Res.*, **2**, 38–55.

Simmons, A., and B. Hoskins, 1978. The life-cycles of some nonlinear baroclinic waves. *J. Atmos. Sci.*, **35**, 414–432.

Thompson, D. W. J., J. M. Wallace, and G. C. Hegerl, 2000. Annular modes in the extratropical circulation. Part II: Trends. *J. Climate*, **13**, 1018–1036.

Vallis, G. K., E. P. Gerber, P. J. Kushner, and B. A. Cash, 2004. A mechanism and simple dynamical model of the North Atlantic Oscillation and annular modes. *J. Atmos. Sci.*, **61**, 264–280.

Watterson, I. G., 2002. Wave-mean flow feedback and the persistence of simulated zonal flow vacillation. *J. Atmos. Sci.*, **59**, 1274–1288.

Watterson, I. G., 2007. Southern 'annular modes' simulated by a climate model: Physical mechanisms and interactions. *J. Atmos. Sci.*, **this issue**.

List of Tables

parameter	default value	description
ΔT_{eq}	60 K	equilibrium profile equator-to-pole temperature difference
k_a	40^{-1} day^{-1}	inverse thermal damping timescale
k_f	1 day^{-1}	inverse momentum damping timescale at surface

TABLE 1: Model parameter definitions and values for the control simulation.

simulation set	horiz. res.	length (days)	ΔT_{eq} (K)	k_a^{-1} (day)	k_f^{-1} (day)	land-sea contrast	topo. (m)
I	T42	6000	30,40,50, 60,70,80,90	40	1	-	-
II	T63	3700	40,60,80	40	1	-	-
III	T42	6000	60	60,40,30	1	-	-
IV	T42	6000	60	40	1.5,1,0.75	-	-
V	T42	9000	40,60,80	40	1	yes	-
VI	T42	9000	40,60,80	40	1	-	1000
VII	T42	9000	40,60,80	40	1	-	2000
VIII	T42	9000	40,60,80	40	1	yes	2000

TABLE 2: Experiments. In each set, one parameter was varied while the others were kept constant, e.g., in set I, we compare 7 simulations of 6000 days, each with a different value of ΔT_{eq}. All simulations were run with 20 evenly spaced σ-levels, and allowed to spin up for 250-300 days before data was collected for the time specified in the third column.

List of Figures

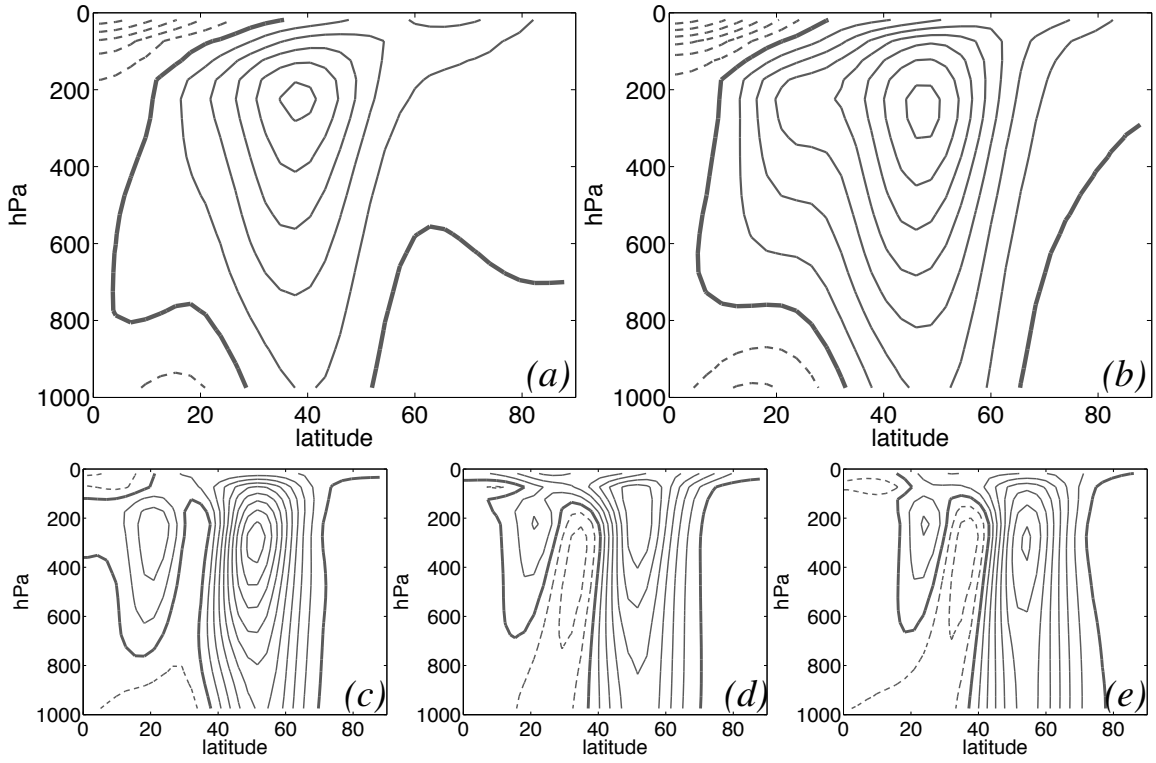

FIGURE 1: (a) and (b): The time and zonal average zonal wind for two simulations from experiment set I. In (a), $\Delta T_{eq} = 40$ and in (b), $\Delta T_{eq} = 80$. (c)-(e): The difference in the time and zonal average zonal winds between two simulations. Panel (c) shows the difference between the simulations shown in panels (b) and (a), in which the equilibrium temperature gradient was varied. Panel (d) shows show the difference between two simulations in experiment set III, where the thermal damping was varied: the winds with $k_a = 30^{-1}$ less those in a simulation with $k_a = 60^{-1}$. Panel (e) shows the difference in winds from two simulations in IV, where the momentum damping was varied: a simulation with $k_f = 1.5^{-1}$ less those in one with $k_f = 0.75^{-1}$. The contour interval is 5 m/s in panels (a) and (b) and 2.5 m/s in panels (c)-(e). Negative contours are dashed and the zero contour is doubled in thickness.

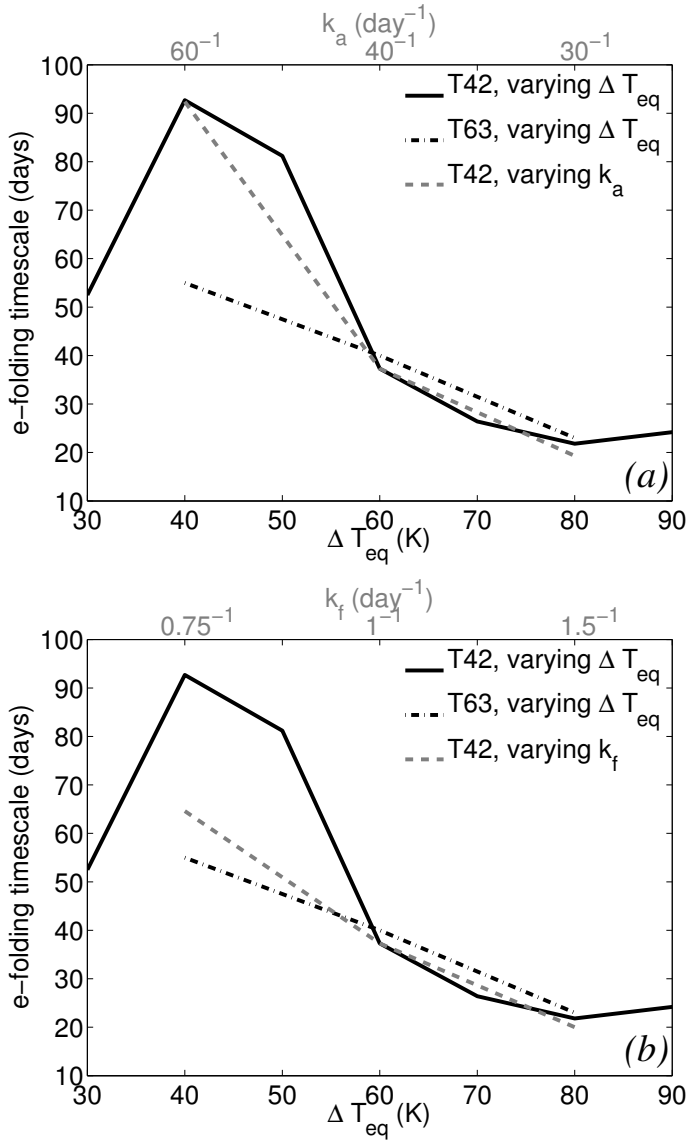

FIGURE 2: The e-folding timescale of the zonal index as function of model parameters. The solid and dot-dashed black curves in both panels illustrate the e-folding timescale as function of ΔT_{eq}, and correspond with the lower x-axis. In (a), the dashed gray curve marks the e-folding timescale as a function of k_a, while in (b) it shows the timescale as a function of k_f. In both cases the values of the damping coefficients are shown on the upper x-axis. In each sensitivity test the other parameters were held constant at their control values, as listed in Table 1.

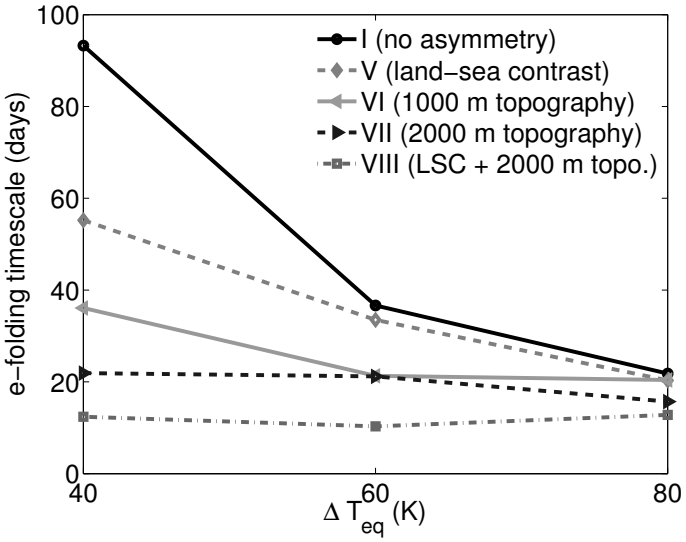

FIGURE 3: The impact of zonally asymmetric forcing and the equilibrium temperature gradient on the e-folding timescale of the annular mode. For experiment sets I and V-VIII, we plot the e-folding timescale of the first EOF of SLP in three simulations with different values of ΔT_{eq}, the equilibrium temperature gradient. In the zonally symmetric simulations of I the first EOF has a perfectly annular structure. With increased zonal asymmetry, in particular the simulations in VIII (where LSC refers to land-sea contrast), the annular mode has an NAO-like zonal structure, with most emphasis in the exit region of the storm track.

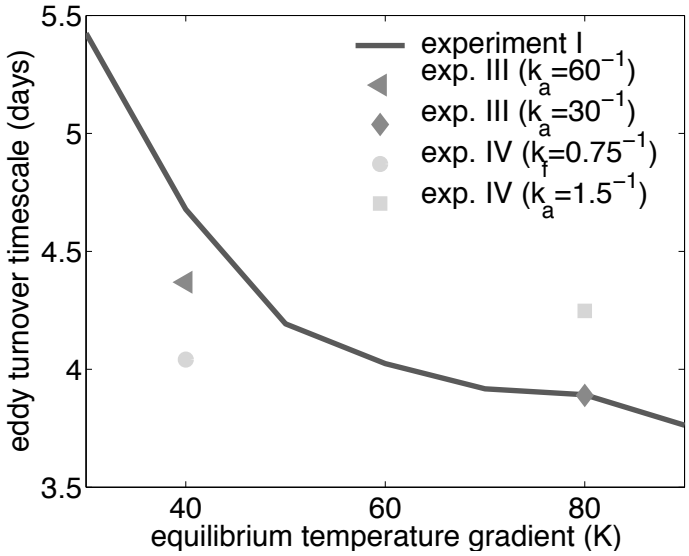

FIGURE 4: The eddy turnover timescale, $L/K^{1/2}$, as a function of the equilibrium temperature gradient, ΔT_{eq}. The eddy kinetic energy, K, increases linearly with the equilibrium gradient, while the eddy length scale is roughly constant. Hence the curve is proportional to $\Delta T_{eq}^{-1/2}$. Values for four other zonally symmetric simulations in experiments III and IV (where k_a and k_f were varied, respectively) are shown for comparison. The points were plotted near the simulation from experiment I that had the most similar climatology and intraseasonal variability.

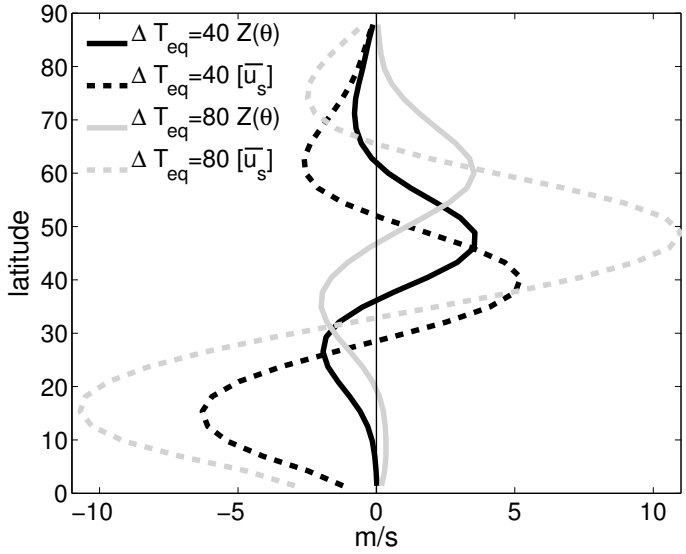

FIGURE 5: The time and zonal average surface ($\sigma = 0.975$) winds, $[\overline{u_s}]$, and the first EOF of $\overline{u_s}$, $Z(\theta)$, for simulations for experiment I with $\Delta T_{eq} = 40$ and 80. Units for the EOF patterns are per standard deviation of their respective zonal indices.

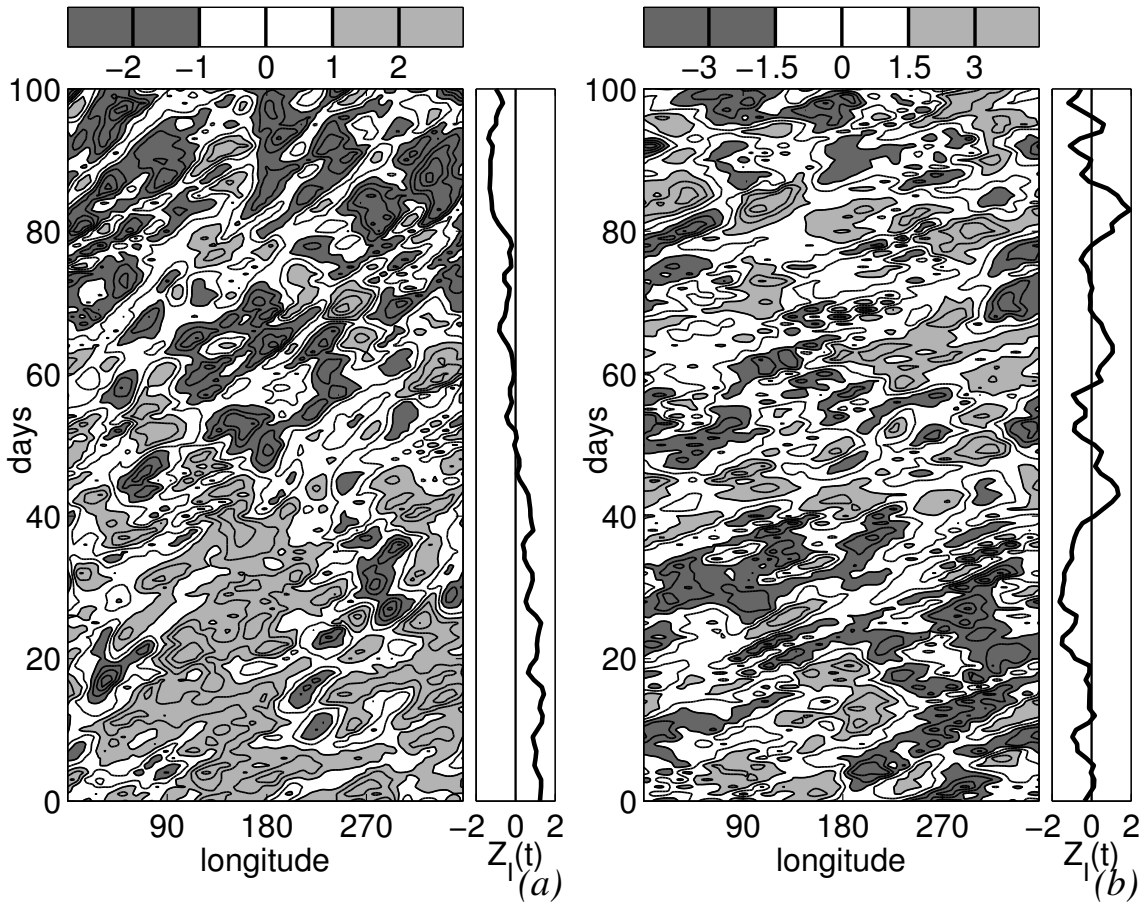

FIGURE 6: Hövmöller diagrams of the dipole index $D_I(t,\lambda)$ for simulations with (a) $\Delta T_{eq} =$ 40 and (b) 80 K. The contour interval is 1 deviation in (a) and 1.5 deviations in (b). The curves on the right show the behavior of the zonal index as a function of time, in units of standard deviations.

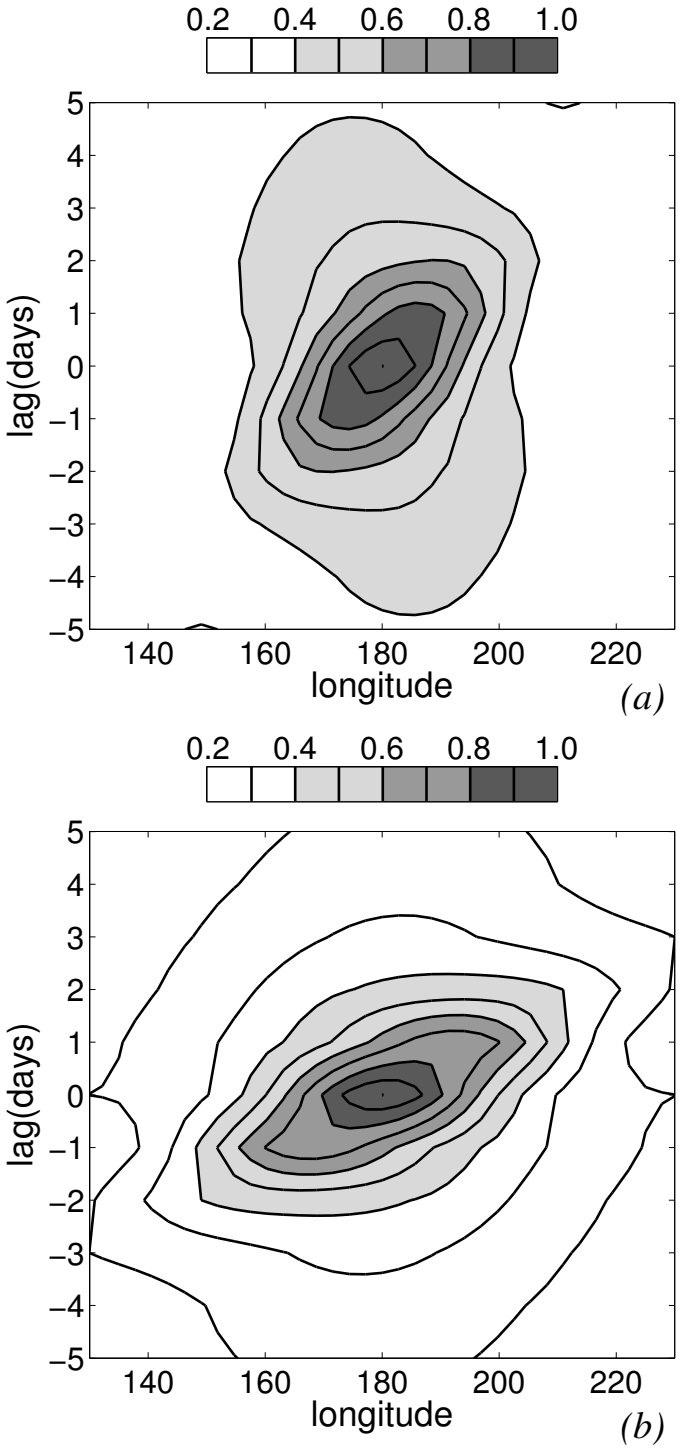

FIGURE 7: The lag-longitude autocorrelation of the dipole index, $D_I(t,\lambda)$, for the simulations with (a) $\Delta T_{eq} = 40$ and (b) $\Delta T_{eq} = 80$. The base longitude for the map is 180°. As noted in the text, the correlation maps at other longitudes are the same with respect to the base point, except for sampling errors. We thus averaged over all longitudes to improve statistics, and the choice of this particular base point was made for plotting purposes.

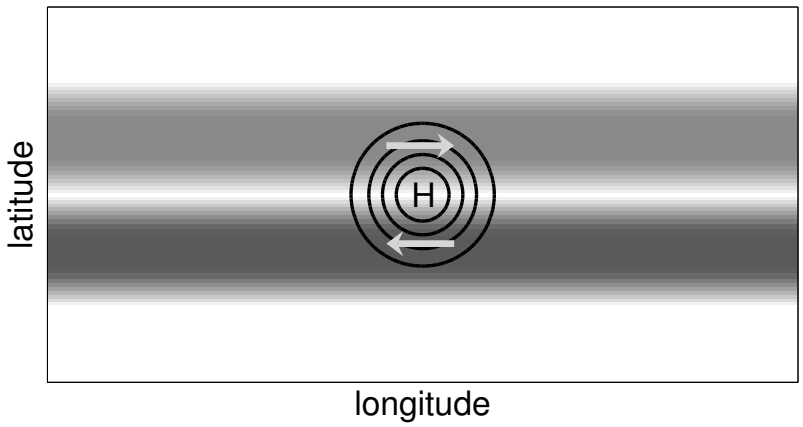

FIGURE 8: A cartoon illustrating the potential for a single eddy to project strongly on the zonal index, or annular mode. The dipole structure of the surface zonal wind is illustrated with positive and negative bands, and the eddy marked by black contours of pressure.

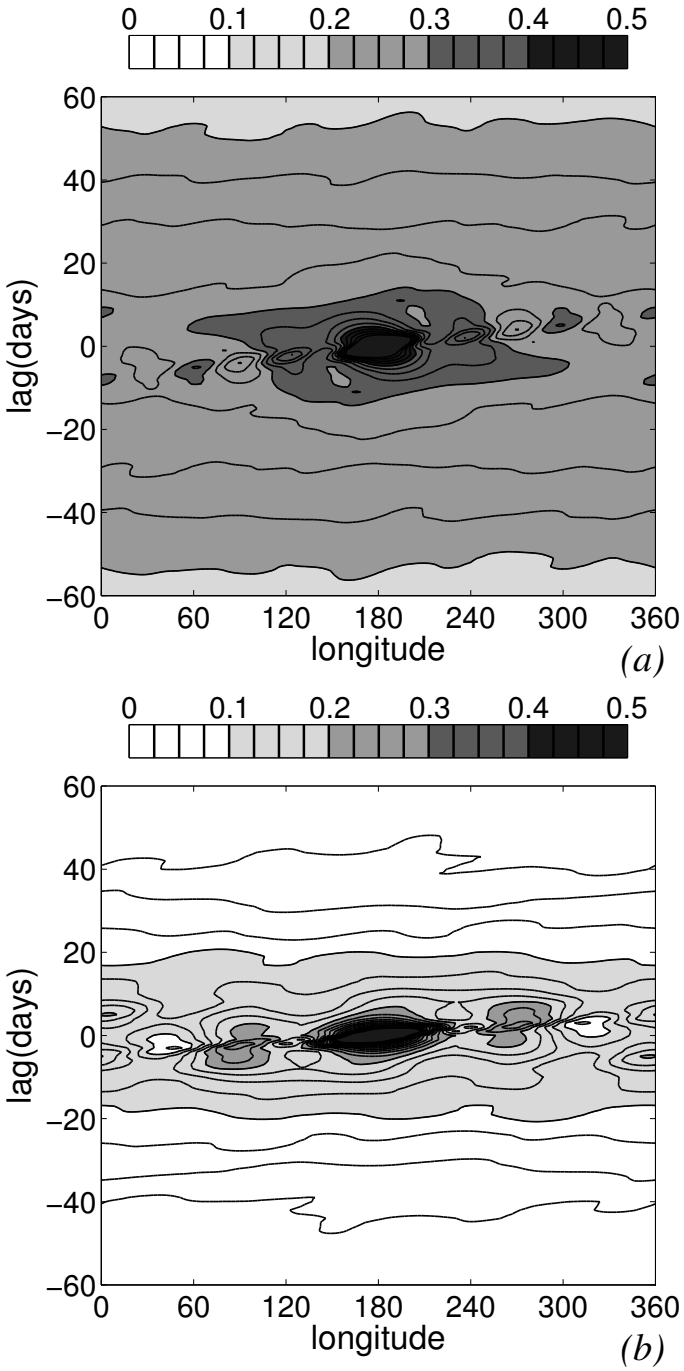

FIGURE 9: Same as Figure 7, but with the range extended to show all longitudes and longer lags, and the scale saturation at 0.4 to focus on the zonally uniform correlations at long lag.

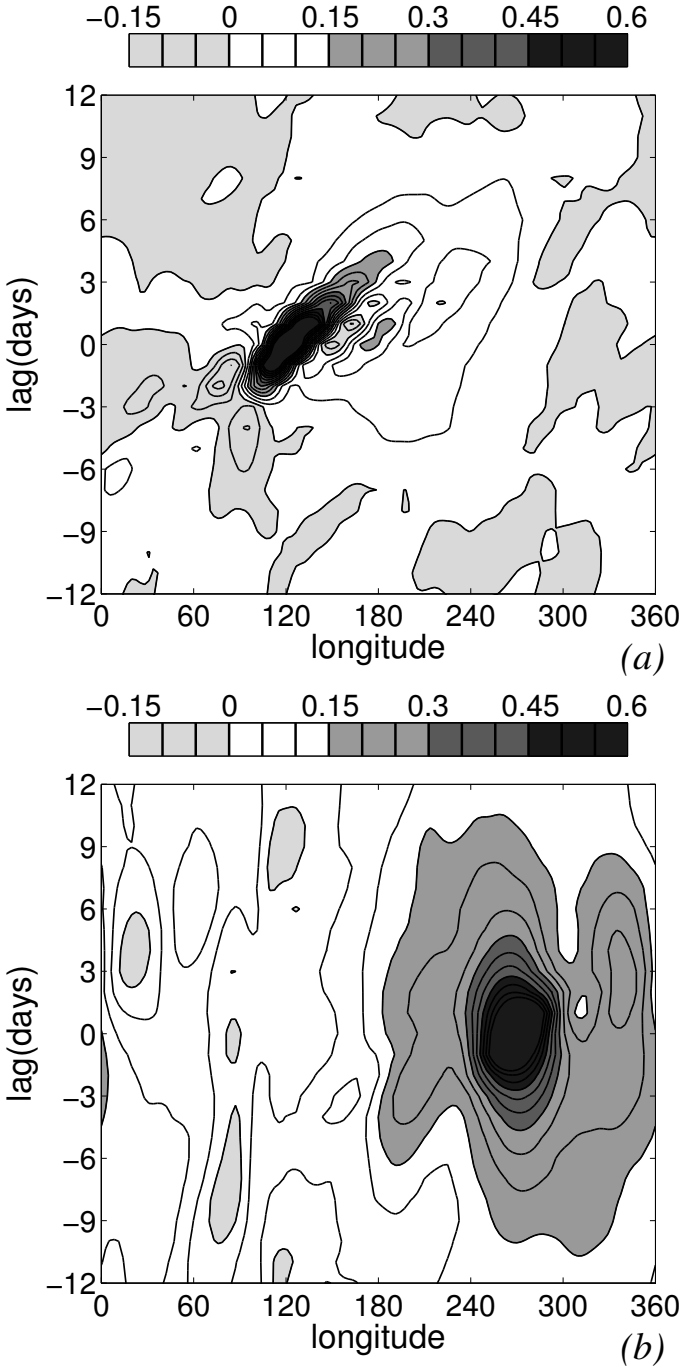

FIGURE 10: Lag-longitude autocorrelation maps from the simulation with $\Delta T_{eq} = 60$ in experiment VIII. The grey scale has been saturated at 0.45, to reveal the large-scale structure. In (a), the base longitude is 120° E, near the entrance to the storm track. In (b), it is 270° E, in the exit region of the storm track where the model's annular mode indicates a maximum in the intraseasonal variability.

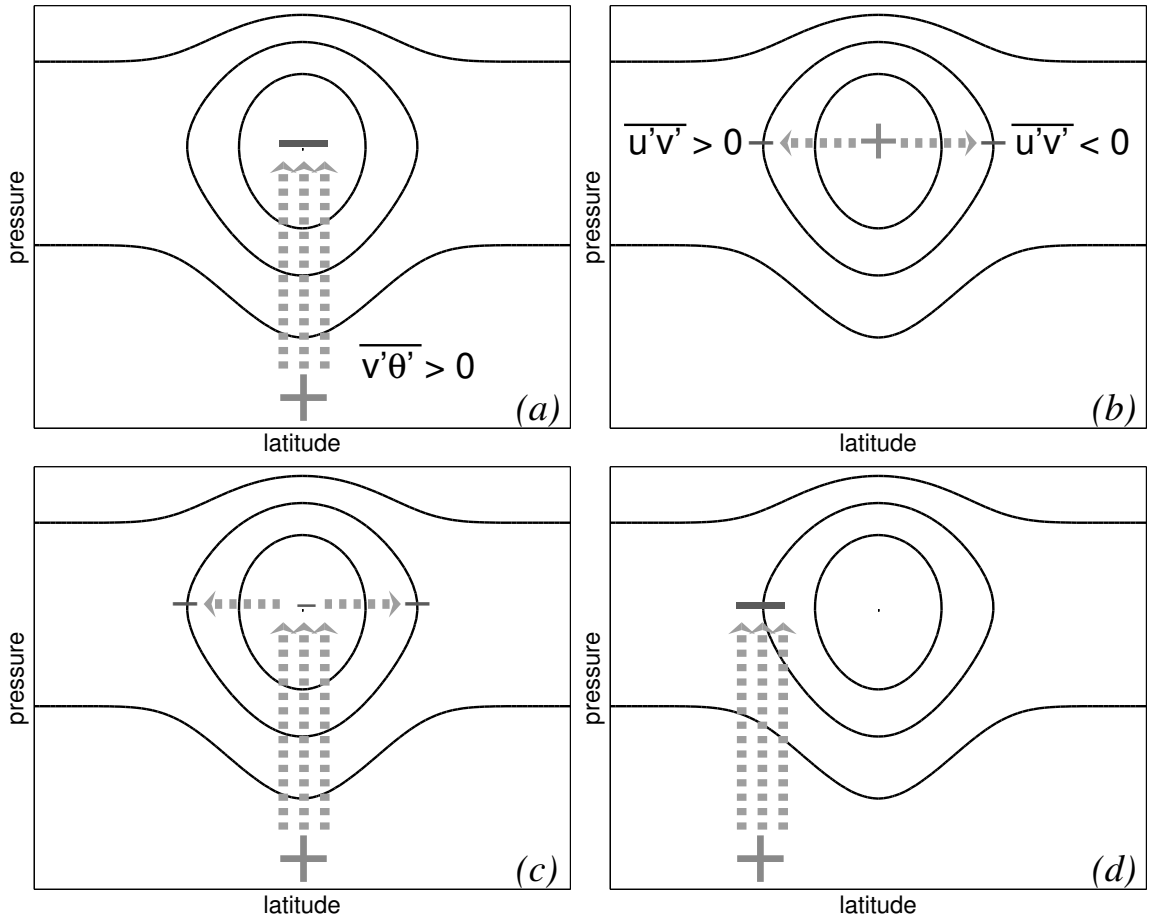

FIGURE 11: A diagram of the eddy mean flow feedback. Solid contours mark the position of the zonal mean winds. Dashed arrows denote the propagation of wave activity, or, equivalently, the direction of Eliassen-Palm (E-P) fluxes. Plus and minus signs indicate divergence and convergence of the E-P fluxes, and so westerly or easterly torque on the mean flow. Panels (a) and (b) break down the impact of eddy heat and momentum fluxes on an eddy formed in the jet core, leading to the net forcing of the flow pictured in (c). Momentum fluxes in upper levels spread the easterly torque over the jet, maintaining the shear in the core. For an eddy generated on the flank of the jet, shown in panel (d), weak upper level winds limit meridional propagation, and the shear tends to be reduced only locally.

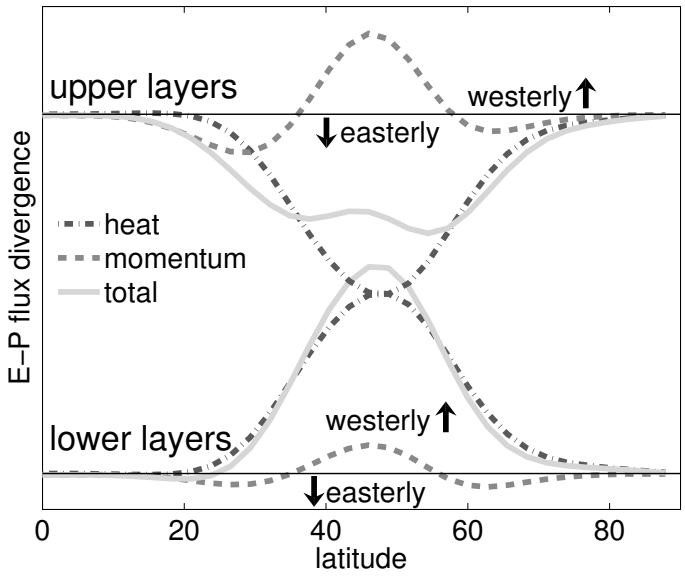

FIGURE 12: The acceleration of the mean flow, $\partial\overline{u}/\partial t$, by the 2-10 day band pass eddies in the control simulation, averaged over all times when the zonal index is neutral, $|Z_I(t)| < 1$. The upper curves show the forcing averaged over the top 500 hPa of the atmosphere, the lower curves the same for the bottom half of the atmosphere. The dashed curves show the acceleration due to eddy momentum fluxes, $-r_0^{-1}(\partial_\theta\,\overline{u'v'} - 2\tan\theta\;\overline{u'v'})$, and the dot-dashed curves that due to eddy heat fluxes, $f\partial_p(\overline{v'\theta'}/\overline{\theta_p})$. The solid curves show the total acceleration, the sum of the two other curves.

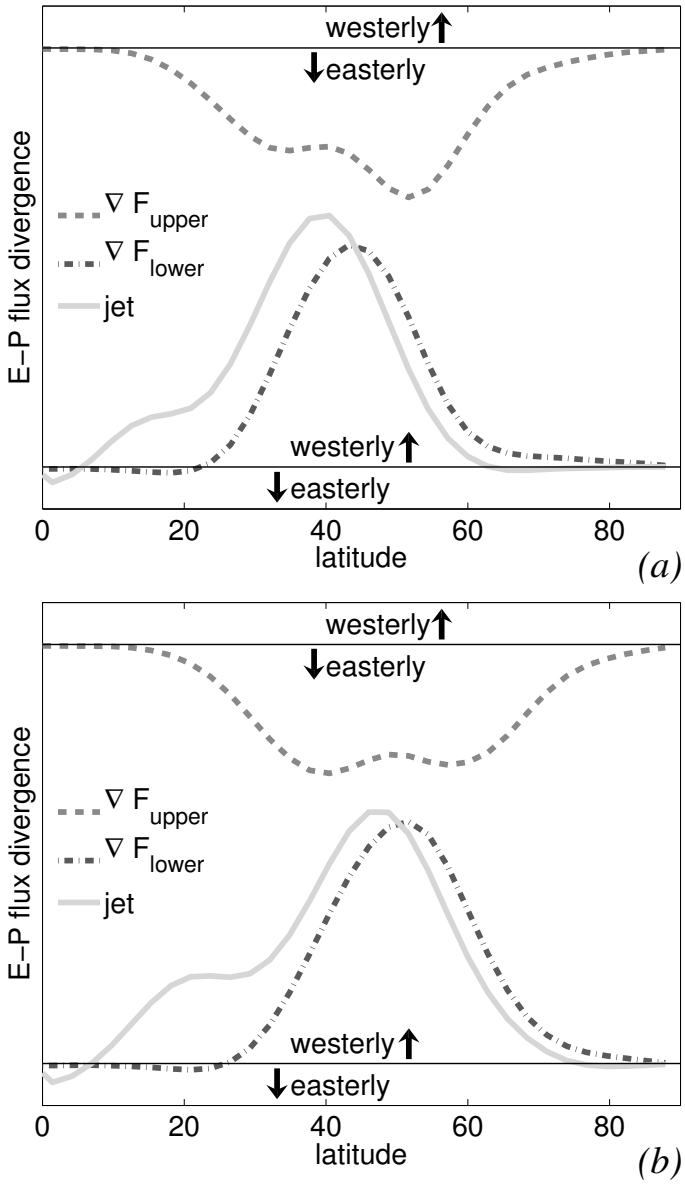

FIGURE 13: Evidence for the eddy-mean flow interaction in the control simulation. Composites based on (a) weak and (b) strong zonal index events, as determined by a threshold of $\pm$ 1 standard deviation of the zonal index $Z_I(t)$. The dot-dashed curves show the acceleration of the zonal average flow, $\nabla \boldsymbol{F}$, by 2-10 day band pass eddies averaged over the lower half of the atmosphere. The torque is westerly at nearly all latitudes. The dashed curves show the acceleration of the upper half of the atmosphere; a negative (easterly) torque. The solid curves show composites of the upper level jet: $\overline{u}$ averaged over the upper half of the atmosphere.